PCCP

The quest to uncover the nature of benzonitrile anion

Journal:	*Physical Chemistry Chemical Physics*
Manuscript ID	CP-ART-11-2019-006484.R1
Article Type:	Paper
Date Submitted by the Author:	28-Dec-2019

Complete List of Authors:	Gulania, Sahil; University of Southern California, Department of Chemistry Jagau, Thomas; Ludwig-Maximilians-Universitat Munchen, Chemistry Sanov, Andrei; University of Arizona, Department of Chemistry and Biochemistry Krylov, Anna; University of Southern California, Department of Chemistry

PCCP

ROYAL SOCIETY OF CHEMISTRY

ARTICLE TYPE

Cite this: DOI: 10.1039/xxxxxxxxxx

The quest to uncover the nature of benzonitrile anion

Sahil Gulania,[a] Thomas-C. Jagau,[b], Andrei Sanov[c], and Anna I. Krylov*[a]

Received Date
Accepted Date

DOI: 10.1039/xxxxxxxxxx

www.rsc.org/journalname

Anionic states of benzonitrile are investigated by high-level electronic structure methods. The calculations using equation-of-motion coupled-cluster theory for electron-attached states confirm earlier conclusions drawn from the photodetachment experiments that the ground state of the anion is the valence $^2B_1$ state, while the dipole bound state lies adiabatically ∼0.1 eV above. Inclusion of triple excitations and zero-point vibrational energies is important for recovering relative state ordering. The computed Franck–Condon factors and photodetachment cross-sections further confirm that the observed photodetachment spectrum originates from the valence anion. The valence anion is electronically bound at its equilibrium geometry, but is metastable at the equilibrium geometry of the neutral. The dipole-bound state, which is the only bound anionic state at the neutral geometry, may serve as a gateway state for capturing the electron. Thus, the emerging mechanistic picture entails electron capture via dipole bound state, followed by non-adiabatic relaxation forming valence anion.

1 Introduction

Benzonitrile (C_6H_5CN) has recently become the first aromatic molecule observed in the interstellar medium using a radio telescope[1]. Its detection in the cold-core Tauras Molecular Cloud 1 (TMC-1) has far-reaching implications as it provides a chemical link for unidentified infrared bands in the interstellar medium. These emission features have long been thought to be due to the polycyclic aromatic hydrocarbons (PAH)[2] and polycyclic aromatic nitrogen heterocycles (PANH)[3]. However, proving the presence of these molecules in the interstellar space has been a challenge for radio-astronomy due to the nonpolar or weakly polar nature of the polycycles combined with the large density of states. Benzonitrile is one of the simplest nitrogen-containing aromatic compounds. As a small molecule with a large dipole moment (> 4 Debye), it does not have the same detection limitations as the polycycles. The observation of benzonitrile in TMC-1 provides the clearest indication to date that larger PAH and PANH species are likely to be present there as well.

The molecular dipole moment also plays an important role in electron capture and anion formation[4–9]. Among the negative ions previously detected in the interstellar medium[10], many are carbon-chain species[11–15], such as $C_{2n-1}N^-$ and $C_{2n}H^-$. In these systems, electron capture by the neutral molecule may involve doorway dipole-bound states[16–21] or dipole-stabilized resonances[22,23]. The large dipole moment of benzonitrile is a predictor of the existence of a dipole-bound state of its anion which may be a precursor for other chemical and photochemical pathways involving negative ions in both the laboratory environments and interstellar space.

The goal of this work is to establish the key electronic properties of benzonitrile, such as its electron affinity (EA) and the nature of electron binding in its anion. Despite several previous investigations, including a direct photoelectron imaging measurement[24], the debate about the very nature of benzonitrile anion is still ongoing. The existence of both dipole-bound and valence states of the anion has been predicted[24,25]. Despite drastically different characters of the respective wave-functions, both types of anions are expected to be weakly bound, with similar electron attachment and detachment energies, making the assignment and interpretation of experimental data a delicate task.

The first measurement of the EA of benzonitrile dates back to 1975[26], when it was indirectly determined to be 0.256(17) eV. Another, also indirect, measurement[27] based on electron capture detection in 1983 yielded a value with a significantly larger uncertainty, 0.26(10) eV, nonetheless in perfect agreement with the earlier determination. Subsequent 1992 experiment indicated that the ground-state anion of benzonitrile could not be observed by electron transmission spectroscopy and hence it was concluded that the anion is bound by a few tenths of an electron-volt[28].

The 2015 photoelectron imaging experiment by Sanov and coworkers[24] yielded the photoelectron spectra and angular distributions for the bare and microsolvated benzonitrile anion. Fig. 1 shows the photoelectron spectra of $C_6H_5CN^-$ and $C_6H_5CN^-\cdot H_2O$

[a] Department of Chemistry, University of Southern California, Los Angeles, California 90089, U.S.A.; E-mail: krylov@usc.edu
[b] Department of Chemistry, University of Munich (LMU), 81377 Munich, Germany
[c] Department of Chemistry and Biochemistry, University of Arizona, Tucson, Arizona 80721, U.S.A.

† Electronic Supplementary Information (ESI) available: relevant Cartesian geometries, basis set details, normal mode analysis. See DOI: 10.1039/cXCP00000x/

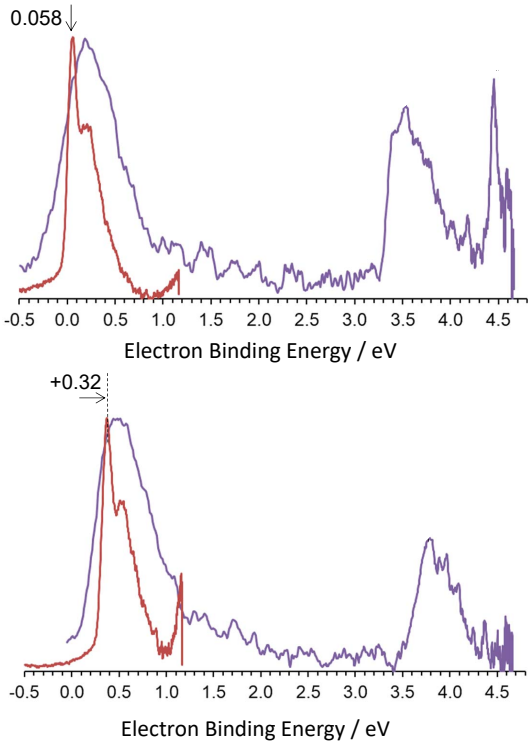

Fig. 1 Photoelectron spectra of $C_6H_5CN^-$ (top) and $C_6H_5CN^-\cdot H_2O$ (bottom) obtained with two different energy photons. Red and blue lines correspond to the spectra obtained with 1.165 eV and 4.661 eV photons, respectively. Reproduced with permission from Ref. 24.

obtained at two different photon energies. The authors reported vertical detachment energy (VDE) of bare $C_6H_5CN^-$ of 0.058(5) eV, while in the $C_6H_5CN^-\cdot H_2O$ cluster the band was blue-shifted by 0.32 eV. The spectra were assigned to the valence anion (VA) of benzonitrile, although a contribution of the dipole-bound state (DBS) could not be ruled out. The authors also calculated the EAs and VDEs for $C_6H_5CN^-$ and $C_6H_5CN^-\cdot H_2O$ using equation-of-motion coupled-cluster (EOM-CC) methods[29–31]. Of particular note, the computed VDE of $C_6H_5CN^-$ (0.047 eV) was in good agreement with the 0.058(5) eV experimental value. The calculations were carried out for the valence state of the benzonitrile anion in which the extra electron occupied a π^*-like (b_1) orbital and the target photodetachment transition corresponded to electron removal from the singly occupied HOMO of the anion. The assignment of the experimental spectrum to the VA of benzonitrile took into account the good agreement between the computed and experimental VDE values. It was additionally supported by the analysis of the photoelectron angular distributions, the Franck–Condon simulation of the low-energy photodetachment band, and the behavior of the band under the microsolvation conditions. However, while concluding that the experimental results could be completely explained by the VA structure of benzonitrile, the authors did not explicitly analyze the DBS.

In a subsequent computational study[25], Adamowicz and co-workers examined the structures and energetics of both the VA and DBS of benzonitrile using the CCSD(T) method (CCSD[32] with perturbative account of triple excitations[33]). They reported[25] the VDE of the DBS of benzonitrile to be 0.019 eV, while claiming that the VA is adiabatically unbound. Although the above VDE did not agree well with the published photoelectron spectra, the authors nonetheless suggested that the experimental spectra of Sanov and co-workers should be attributed to the DBS, rather than the VA of benzonitrile.

In the present study, we resolve the ambiguity created by the above conflicting conclusions. We report high-level calculations showing that the photodetachment transitions observed by Sanov and co-workers are indeed attributed to the valence anion, but also discuss the possibility that the DBS may serve as a doorway state in the formation of the VA. This route is easily accessible in benzonitrile and therefore future detection of its anion in ISM should be anticipated.

2 Theoretical methods

The EOM-CC approach[29–31,34–41] provides an efficient and robust framework for computing a variety of electronic states in closed- and open-shell species. Different variants of EOM-CC enable access to different types of target electronic states, such as electronically excited, electron attached or ionized states. The EOM-CC wave-function has the following form:

$$|\Psi\rangle = Re^T |\Phi_0\rangle, \tag{1}$$

where the linear EOM operator R acts on the reference CC wave-function, $e^T|\Phi_0\rangle$. The operator T is an excitation operator satisfying the CC equations for the reference state

$$\langle\Phi_\mu|\bar{H}|\Phi_0\rangle = 0, \tag{2}$$

where Φ_μ are the μ-tuply excited determinants and $\bar{H} = e^{-T}He^T$. In EOM-CCSD, the CC and EOM operator are truncated as follows[32,38]:

$$T \approx T_1 + T_2, \qquad R \approx R_0 + R_1 + R_2, \tag{3}$$

where T_1 and T_2 are single and double excitation operators, 1-hole-1-particle ($1h1p$) and 2-holes-2-particles ($2h2p$):

$$T_1 = \sum_{ia} t_i^a a^\dagger i, \qquad T_2 = \frac{1}{4}\sum_{ijab} t_{ij}^{ab} a^\dagger b^\dagger ji. \tag{4}$$

Different variants[29–31] of EOM-CC are defined by different choices of the reference state and the type of EOM operators R. For example, by choosing the reference as a neutral state and R_1 and R_2 as $1h$ and $2h1p$ operators, one can describe ground and excited states of the cation. This strategy was used by Sanov and co-workers[24], who computed VDE by EOM-IP-CCSD from the open-shell VA state of benzonitrile. A more balanced treatment of open-shell anionic states is afforded by the EOM-EA-CCSD variant[42] in which the reference is a neutral closed-shell state and R_1 and R_2 are of $1p$ and $1h2p$ type, as illustrated in Fig. 2:

$$R_1 = \sum_i r^a a^\dagger, \qquad R_2 = \frac{1}{2}\sum_{iab} r_i^{ab} a^\dagger b^\dagger i. \tag{5}$$

Here we characterize the VA and DBS of benzonitrile by EOM-EA-CCSD starting from the ground state of the neutral benzoni-

trile; in these calculations VDE is obtained as the energy difference between the EOM-EA-CCSD and CCSD states. The accuracy of EOM-CC can be systematically improved by including higher-level of excitations in T and R, up to the exact limit. Here we account for the effect of triple excitations by using perturbative correction, i.e., the EOM-EA-CCSD(T)(a)* method[43,44].

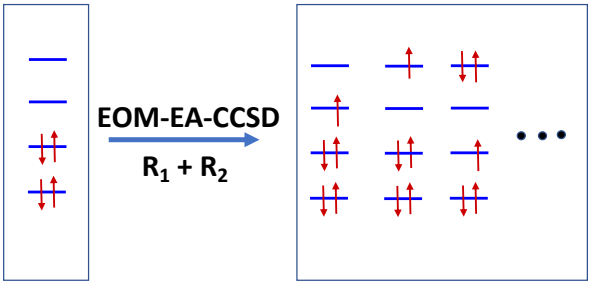

Fig. 2 EOM-EA target configurations generated from a closed-shell reference state. The first two configurations are $1p$ ones and the third one is $2p1h$.

The EOM amplitudes and the corresponding energies are found by diagonalizing the similarity transformed Hamiltonian, $\bar{H}$. Since $\bar{H}$ is a non Hermitian operator, its left and right eigenstates are not identical but can be chosen to form a biorthonormal set.

$$\bar{H}R|\Phi_0\rangle = ER|\Phi_0\rangle, \tag{6}$$

$$\langle\Phi_0|L\bar{H} = \langle\Phi_0|LE, \tag{7}$$

$$\langle\Phi_0|L^M R^N|\Phi_0\rangle = \delta_{MN}, \tag{8}$$

where M and N denote the M^{th} and N^{th} EOM states and

$$L = L_1 + L_2 = \sum_a l_a a + \frac{1}{2}\sum_{iab} l^i_{ab} i^\dagger ba. \tag{9}$$

The left and right amplitudes are found by diagonalizing the corresponding matrix representation of $\bar{H}$. For energy calculations, right eigenstates are sufficient, but for property calculations, such as Dyson orbitals[45], both left and right eigenstates need to be computed.

Dyson orbitals are reduced quantities defined as the overlap between an initial N-electron and final $N-1$-electron states:

$$\phi^{\text{Dyson}}_{if}(x_1) = \sqrt{N}\int \Psi^N_i(x_1,x_2,\ldots,x_N)\Psi^{N-1}_f(x_2,\ldots,x_N)dx_2\ldots dx_N. \tag{10}$$

Because Dyson orbitals enter the expressions of various experimental observables, such as photoionization/photodetachment cross sections[46,47], they can be interpreted as correlated states of the ejected/attached electron. Thus, Dyson orbitals provide a basis for a rigorous extension of molecular orbital theory to many-body correlated wave functions[45,48,49]. Here we compute Dyson orbitals using the CCSD (as Ψ^{N-1}_f) and EOM-EA-CCSD (as Ψ^N_i) wave functions of the neutral and of the anion, respectively.

3 Computation details

As outlined above, we characterized valence and dipole-bound states of the benzonitrile anion by EOM-EA-CCSD using the neutral CCSD reference. Core electrons were frozen in all correlated calculations. Our primary focus is on the relative energetics of the neutral, VA, and DBS. For negative ions, VDE is defined as energy gap between the ground-state energy of the anion and the corresponding neutral molecule, both at the equilibrium geometry of the anion ($\mathbf{R}_A$):

$$\text{VDE} = E_N(\mathbf{R}_A) - E_A(\mathbf{R}_A). \tag{11}$$

Analogously, vertical attachment energy (VAE) is computed at the equilibrium geometry of the ground-state neutral molecule ($\mathbf{R}_N$):

$$\text{VAE} = E_A(\mathbf{R}_N) - E_N(\mathbf{R}_N). \tag{12}$$

The electronic part of the adiabatic electron affinity (AEA_{ee}) is defined as the energy difference between the ground-state energy of the anion at its equilibrium geometry and the ground-state energy of the neutral at its equilibrium geometry:

$$\text{AEA}_{ee} = E_N(\mathbf{R}_N) - E_A(\mathbf{R}_A). \tag{13}$$

The difference between AEA_{ee} and VDE arises due to structural differences between the anionic and neutral states. Thus, the two quantities are expected to be the same for DBS but not for VA whose structure differ substantially from that of the neutral.

To obtain the relative ordering of the anionic states and to compare with the experimental photodetachment onset, we also computed AEA, which includes zero-point energy (ZPE) differences between the anion and the neutral states:

$$\text{AEA} = \text{AEA}_{ee} + \Delta\text{ZPE}. \tag{14}$$

In calculations of energetics, we used the geometry of the neutral and VA states optimized by CCSD/aug-cc-pVTZ and EOM-EA-CCSD/aug-cc-pVTZ, respectively. Both structures are of C_{2v} symmetry. As is well documented in the literature[4,5], the shape of potential energy surfaces of dipole-bound anions are very similar to the respective structures of the neutral species because the extra electron resides largely outside the molecular core. Thus, the energies of DBS were computed at the geometries of the neutral benzonitrile. Triples corrections to the VDE and AEA of the VA were computed with EOM-EA-CCSD(T)(a)* method[43,44] using aug-cc-pVTZ. We assume that the effect of triples cancels out for the DBS, because the unpaired electron does not participate in the bonding.

Because of their structural similarity, we also expect vibrational frequencies of the neutral and DBS to be similar, giving rise to $\Delta\text{ZPE}\approx 0$. ZPEs of the neutral and the VA states were computed within the harmonic approximation with CCSD and EOM-EA-CCSD using aug-cc-pVDZ and resolution-of-the-identity (RI) approximation[50,51] with the matching basis set (ri-aug-cc-pVDZ), at the geometries optimized at the same level of theory. The computed structures and normal modes were used to compute the Franck–Condon factors within parallel-mode double-harmonic approximation using the *ezSpectrum* software[52]; these calculations used T=300 K. To further elucidate putative contributions of the DBS to the spectra, we computed photoelectron cross sections using EOM-EA-CCSD Dyson orbitals and the *ezDyson* software[53].

To correctly describe DBS, large basis sets with additional sets of diffuse functions are needed. We used the aug-cc-pVTZ basis augmented with several extra sets of diffuse functions added to each atom, with the exponents obtained following the same procedure as in our previous studies[23,54–57]; the details are provided in the SI. Our preliminary calculations monitoring the convergence of the VAE of the DBS showed that the results converge with the aug-cc-pVTZ+6s3p(3s) basis. Here, "6s3p" refers to the additional diffuse functions placed at the heavy atoms and "(3s)" to those placed at the hydrogen atoms. Below we report the energetics of the bare benzonitrile anion obtained with aug-cc-pVTZ+6s3p(3s). For the $C_6H_5CN^-\cdot H_2O$ complex, the VEA of the DBS converged with the aug-cc-pVTZ+4s4p(4s) basis. Thus, for the benzonitrile-water complex, we report energetics obtained with aug-cc-pVTZ+4s4p(4s).

All electronic structure calculations were performed using the Q-Chem package[58,59]. Below we report symmetry labels using Mulliken's convention[60]. Basis sets, relevant Cartesian coordinates, and vibrational frequencies are given in the SI.

4 Results and discussion

4.1 The benzonitrile anion

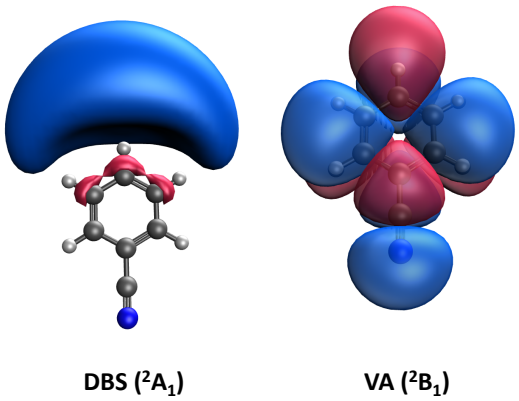

Fig. 3 Dyson orbitals for the two lowest electronic states of the benzonitrile anion, $^2A_1$ and $^2B_1$, computed at the respective optimized geometries. Isovalue 0.007.

Fig. 3 shows Dyson orbitals of the two lowest states of the benzonitrile anion, $^2A_1$ and $^2B_1$. The shape of the orbitals identifies the former as DBS and the latter as VA. In the VA state, the unpaired electron resides on a relatively compact π^*-like orbital of b_1 symmetry, giving rise to the $^2B_1$ state. The Dyson orbital for the DBS is a diffuse *s*-like orbital located on the opposite end of the cyano-group, giving rise to the $^2A_1$ state. The DBS is supported by the large dipole moment of benzonitrile, 4.57 Debye (CCSD/aug-cc-pVTZ).

Fig. 4 shows the schematic energy diagram of the neutral benzonitrile and the two anionic states. The energies shown in the figure are our best estimates of AEAs (EOM-EA-CCSD/CCSD with triples corrections, plus ZPE); the contributions of different components is given in Table 1. The present EOM-EA-CCSD calculations reveal that at the neutral's equilibrium geometry ($\mathbf{R}_N$), the

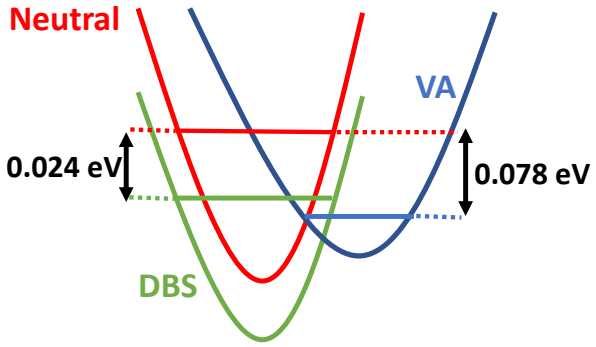

Fig. 4 Schematic representation of the energy levels of the neutral, valence and dipole-bound anionic states of benzonitrile (see text). Note that the VA adiabatically drops below the neutral and the DBS due to zero-point energy.

VA state is electronically unbound, and the only bound anionic state is the DBS, with VEA of 0.024 eV. This finding is consistent with the corresponding results of Adamowicz and co-workers[25], who reported VDE of the DBS to be 0.019 eV with CCSD(T). However, at the optimized geometry of the valence anion, both the DBS and VA are (vertically) bound by 0.026 eV and 0.064 eV, respectively. The latter value is in excellent agreement with the experimental VDE of 0.058(5) eV, previously assigned to the VA[24]. We note that this value is a significant improvement over the corresponding EOM-IP-CCSD value of 0.047 eV, which was obtained using a less balanced protocol based on the open-shell anionic reference and a smaller basis set[24].

Considering only the electronic energies (computed with EOM-EA-CCSD), the DBS minimum is 0.139 eV below the minimum of the VA and the VA is adiabatically unbound (as indicated by the negative AEA_{ee}). However, the ZPE correction makes the VA adiabatically bound by 0.011 eV. A relatively large effect of ΔZPE (0.126 eV) favoring the VA can be easily rationalized by the shapes of the respective Dyson orbitals (Fig. 3): because the electron is attached to the π^* orbital, the vibrational modes of the anion become softer, thus lowering the magnitude of ZPE relative to the neutral. The mode that is most affected by electron attachment is the butterfly mode. The frequency of this mode softens by $\sim$170 cm^{-1} upon electron attachment, which is clearly illustrated in Fig. 5 by the reduction of the curvature of the potential energy profile. The frequencies are given in Table SI in the SI.

The inclusion of perturbative triple excitations increases the attachment energy of the VA by 0.068 eV. Thus, the VA is adiabatically more stable than the DBS when both triple excitations and ZPE are taken into account. Table 1 summarizes the key energetics and Fig. 4 presents the results graphically.

Fig. 4, which shows the relevant energy levels of benzonitrile and its anion, highlights that the VA is bound by 0.078 eV relative to the ground state of the neutral and is 0.054 eV more stable adiabatically than the DBS. However, at the geometry of the neutral, the VA is above the DBS and is electronically unbound. Thus, the DBS may act as a doorway for the VA formation. In this mechanism, the electron is first captured by benzonitrile at its neutral geometry, forming the DBS anion, followed by a non-adiabatic

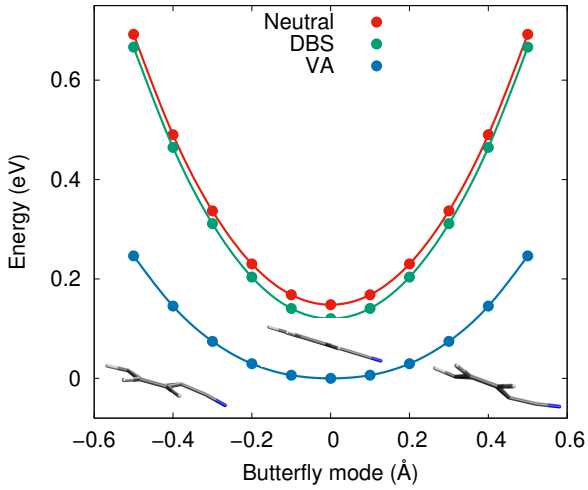

Fig. 5 Potential energy curves along the butterfly mode for VA, DBS, and the neutral, showing the relaxation of VA. Energies along the scan are computed with EOM-EA-CCSD/aug-cc-pVDZ+6s3p(3s). The scan was generated by taking the displacement along the butterfly normal mode of the anion (mode #2 of 209.18 cm^{-1}).

Table 1 Attachment and detachment energies (in eV) for valence ($^2B_1$) and dipole-bound ($^2A_1$) anion of benzonitrile.

State	VAE[a]	VDE[a]	AEA^a_{ee}	ΔZPE[b]	Δ(T)[c]	AEA[d]
$^2A_1$	-0.0240	-	0.0240	∼0	∼0	0.024
$^2B_1$	NB[e]	0.0639	-0.1150	0.1256	0.0677	0.078

[a] EOM-EA-CCSD/aug-cc-pVTZ+6s3p(3s).
[b] RI-CCSD/RI-EOM-EA-CCSD and aug-cc-pVDZ for the VA.
[c] EOM-EA-CCSD(T)(a)*/aug-cc-pVTZ for the VA.
[d] AEA including ΔZPE and triples correction.
[e] Electronically not bound.

transition to the more stable VA state.

4.2 The $C_6H_5CN^-\cdot H_2O$ complex

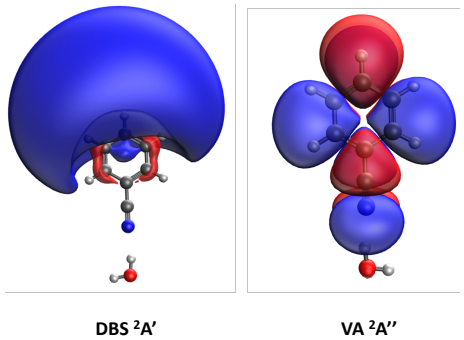

Fig. 6 Dyson orbitals for the two lowest electronic states of the $C_6H_5CN^-\cdot H_2O$ complex, $^2A'$ and $^2A''$, computed at the respective optimized geometries. Isovalue 0.007.

In the $C_6H_5CN^-\cdot H_2O$ complex, the water molecule forms a hydrogen bond with the cyano group, only weekly perturbing the electronic structure of the benzonitrile core. The electronic states of the anion appear to be very similar to those of the bare benzonitrile, as one can clearly see from the Dyson orbitals shown in Fig. 6. However, microsolvation affects the energetics of the states. At the neutral's geometry, the DBS($^1A'$) and VA($^1A''$) are vertically bound by 0.066 eV and 0.054 eV, respectively. The detachment energy for VA increases approximately tenfold, up to 0.457 eV at the optimized geometry of the VA. Adiabatically, the DBS and VA are bound by 0.066 and 0.169 eV, respectively.

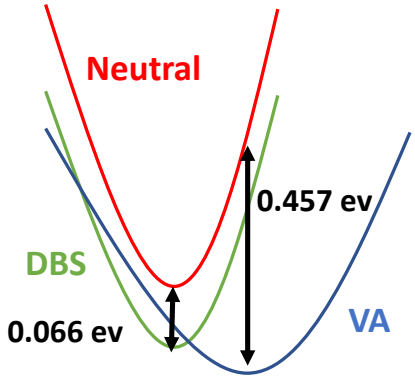

Fig. 7 Schematic representation of the neutral, valence anion, and dipole-bound states of the benzonitrile-water complex.

Fig. 7 shows the relevant state ordering in this complex. Here, the ZPE also makes the VA more bound, but the effect is small, relative to the VDE itself. The computed VDE agrees with the experimental electron detachment energies, confirming that electron detachment happens from the VA. One crucial experimental observation is that the detachment energy increases by 0.32 eV upon addition of water relative to the bare benzonitrile. This value is in good agreement with the 0.39 eV increase in VDE predicted by theory.

Table 2 Attachment and detachment energies (in eV) for the valence ($^1A''$) and dipole-bound ($^2A'$) states of the benzonitrile-water complex.

State	VAE[a]	VDE[a]	AEA^a_{ee}
$^2A'$	-0.0661	-	0.0661
$^2A''$	-0.0535	0.4566	0.1690

[a] EOM-EA-CCSD/aug-cc-pVTZ+4s4p(4s)

4.3 Photodetachment spectra

The computed energetics of the bare benzonitrile suggest that the VA species are dominant even at room temperature (300 K), as shown in Fig. 8. The much larger gap between the VA and DBS in the microsolvated benzonitrile makes the presence of the DBS in $C_6H_5CN^-\cdot H_2O$ highly improbable. In this section, we analyze Franck–Condon factors and photodetachment cross sections for the VA and DBS, to further confirm our assignment.

Using the geometries of the anion and neutral forms of benzonitrile, we computed the Franck–Condon factors for the photodetachment from the VA state and compared them with the experimental spectrum in Fig. 9. The spectra show broad vibrational progression. The analysis of the computed Franck-Condon

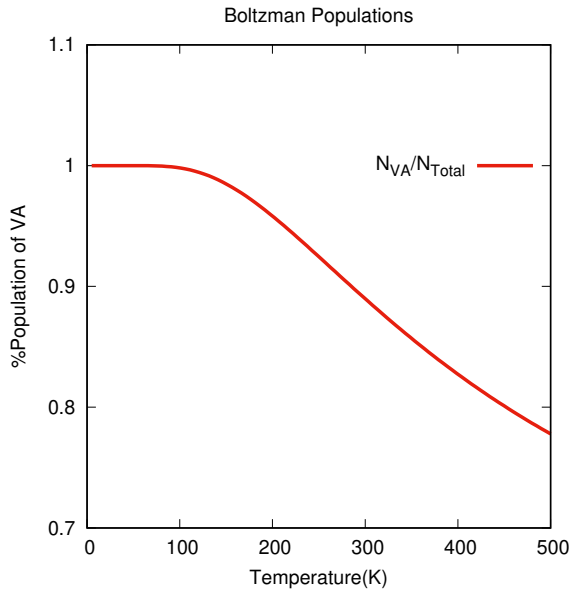

Fig. 8 Ratio of the Boltzmann population of VA (N_{VA}) relative to the total population (N_{total}) as a function of temperature.

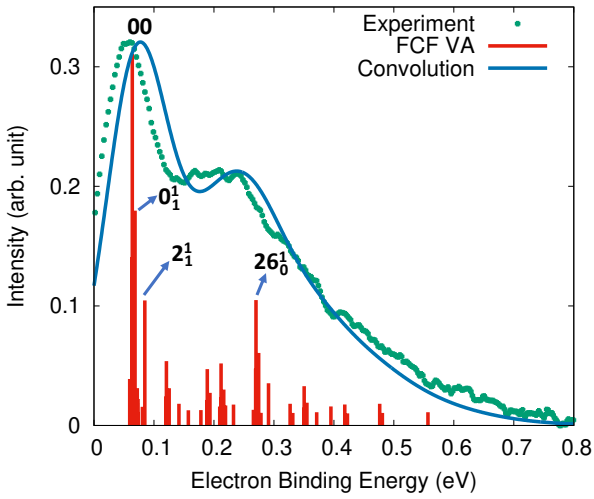

Fig. 9 Computed photoelectron spectrum for the VA and the experimental spectrum obtained by Sanov and co-workers[24]. In the computed spectrum, the Franck-Condon factors were convoluted with gaussians of width 0.05 eV.

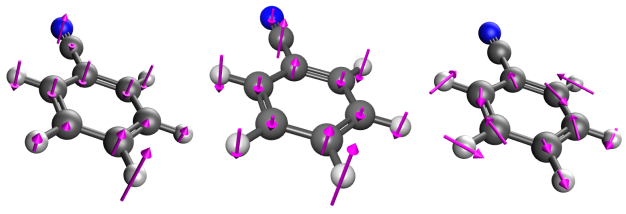

Fig. 10 Franck-Condon active modes: #0 (out-of-plane), #2 (butterfly), and #26 (ring breathing).

factors (Table 3) reveals three dominant modes: ring-breathing mode (#26), butterfly mode (#2), and another soft out-of-plane mode (#0). Symmetric ring-breathing mode is active because of the structural changes between the neutral and the anion along this coordinate, whereas non-symmetric vibrations (modes #0 and #2) give rise to noticeable Franck-Condon factors because of the large change in harmonic frequencies. The frequencies are shown in Table SI of the SI and the modes are shown in Fig. 10. The character of the Franck-Condon modes is consistent with the detachment from the antibonding π^* orbital (Fig. 3, right panel).

As the formation of the DBS of the anion does not lead to a significant change in geometry, the detachment from DBS would result in the sharp 00 transition with no vibrational structure. Thus, the observed vibrational structure in the measured photodetachment spectrum also supports the conclusion that the observed photoelectron spectra must be attributed to the VA rather than the DBS.

Table 3 Peak positions and assignments for the photoelectron spectrum of $C_6H_5CN^-(^1A_1 \leftarrow ^2B_1)$.

Energy (eV)	Intensity (arb. units)	Vibration
0.0634	0.1406	1_1^1
0.0639	0.3106	00
0.0684	0.1797	0_1^1
0.0847	0.1046	2_1^1
1.2701	0.1049	26_0^1

Extending the same argument to the $C_6H_5CN^-\cdot H_2O$ complex, the VA is expected to show a similar Franck–Condon progression in the photoelectron spectra. In the experiment with 1.165 eV photons, both $C_6H_5CN^-$ and $C_6H_5CN^-\cdot H_2O$ indeed show similar Franck–Condon envelops. This observation strongly suggests that the observed photoelectron spectra for both $C_6H_5CN^-$ and $C_6H_5CN^-\cdot H_2O$ correspond to the detachment from VA.

To assess whether possible contributions from the DBS to photoelectron spectra are not seen in the experiment due to potentially low cross section, we also computed absolute photodetachment cross sections using Dyson orbitals and *ezDyson* software[53]. Different orbital characters of DBS and VA result in different trends in the computed cross sections. The absolute cross sections for the two anionic states are shown in Fig. S2 of SI. Fig. 11 shows the dependence of ratio of the two cross sections as a function on the photon energy. The results reveal that at low photon energy the DBS photodetachment cross section is 100 times higher than that of VA. At the 1.165 eV photon energy, corresponding to the experimental spectrum shown in Fig. 9, our calculations predict $\sigma_{DBS}/\sigma_{VA} = 4.65$ (see the inset Fig. 11). Taking this ratio value and estimating the relative intensity of DBS photodetachment at this energy as

$$\mathbf{I}_{DBS} = \mathbf{I}_{VA} \times \frac{\sigma_{DBS}}{\sigma_{VA}} \qquad (15)$$

one can compute the Franck–Condon spectra for an arbitrary mixture of DBS and VA. Fig. 11 shows such a spectrum for an equal mixture of the two anionic states. The sharp threshold peak due to the DBS has a very high relative intensity, dwarfing the Franck-Condon envelope due to the VA. This shows that if the population of the DBS were significant, the first sharp peak in the photo-

electron spectrum would be attributed to DBS. However, the very similar first peak in the $C_6H_5CN^-{\cdot}H_2O$ spectrum (Fig. 1, bottom) should definitely be attributed to VA, based on the energetics shown in Fig. 7. Disregarding the 0.32 eV band shift, the $C_6H_5CN^-$ and $C_6H_5CN^-{\cdot}H_2O$ spectra in Fig. 1 are indeed very similar, strongly suggesting that the electronic character of the core anion should be the same in both cases. This comparison supports the argument that the first peak observed in the experimental spectra of both $C_6H_5CN^-$ and $C_6H_5CN^-{\cdot}H_2O$ originates from the VA. If the DBS were involved, it would contributed more prominently (with a sharp threshold peak) to the spectrum of the unsolvated anion, compared to the micro-hydrated species, overpowering the Franck-Condon features from the VA.

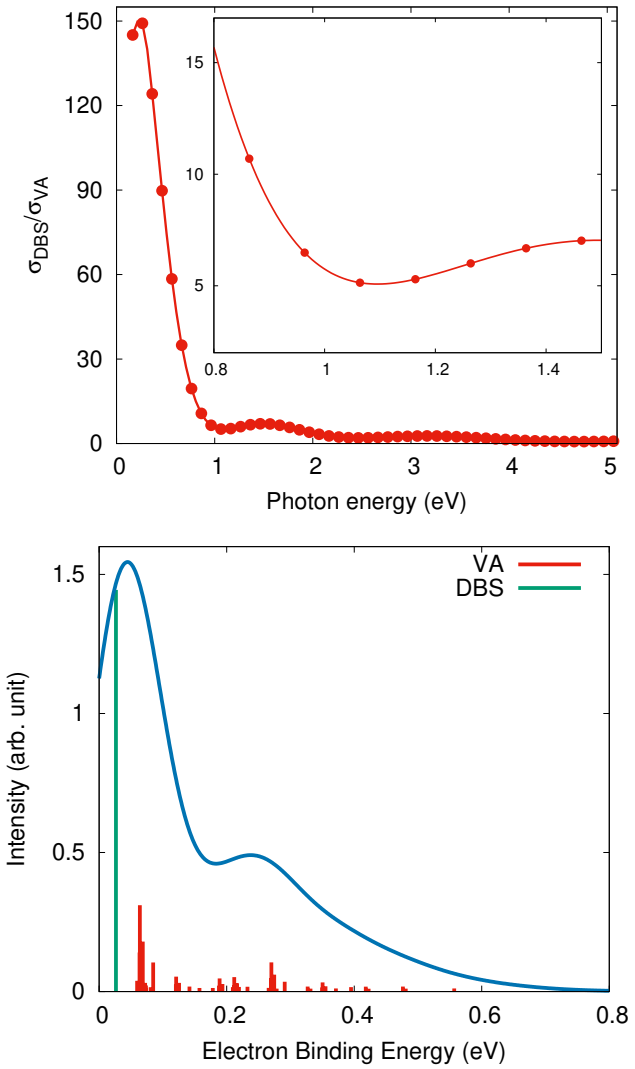

Fig. 11 Top: Ratio of the cross sections (DBS versus VA) for electron detachment from the benzonitrile anion. Bottom: Convolution of the Franck–Condon factors using Eq. (15) with gaussian (width=0.05 eV) and assuming equal populations of the DBS and VA.

A similar interplay between the VA and DBS was observed in uracil[61,62]. An experimental study by Bowen *et. al*[63] was able to distinguish between the DBS and VA in uracil. The photoelectron spectrum of the uracil anion shows a strong narrow single peak at 93 meV. The absence of the Franck–Condon progression indicated negligible structural changes from the anion to the neutral, which is characteristic of DBS. Using argon and krypton as solvents did not affect the narrow peak, but when xenon was used as solvent, the spectra changed dramatically. This behavior was attributed to the polarization effect of xenon, which resulted in breaking the symmetry of the molecule and stabilizing the VA. Using more polar solvent such as H_2O resulted in complete disappearance of the DBS peak.

The behavior of the benzonitrile anion differs from that of uracil in several respects. First, the Franck–Condon features are observed in the photoelectron spectrum with no solvent present. Second, no additional sharp peaks, which could be attributed to the DBS, are seen in the photodetachment of the unsolvated anion, as compared to the micro-solvated species. Third, the VA of benzonitrile is adiabatically more stable than the DBS. Thus, the DBS may act as a doorway to capture the electron, subsequently transferring the population into the VA upon the collisional relaxation of the anion. Since the cross sections for photodetachment are equal to the cross sections of the reverse process, radiative electron attachment, the large value of the cross section for DBS further supports that electron capture directly into this state may be efficient.

5 Conclusion

CCSD and EOM-EA-CCSD calculations of the electronic states of benzonitrile and its anion reveal that although, in terms of electronic energies the VA is adiabatically above the neutral state, the respective ZPE-corrected levels reverse the state ordering, making the VA bound. The inclusion of triples corrections further stabilizes the VA state relative to the neutral and DBS. The computed energetics are in excellent agreement with the experimental values reported in earlier work[24]. The computed Franck–Condon factors provide further support to the assignment of the ground state of the benzonitrile anion as the valence-bound anion, $^2B_1$, rather than dipole-bound state ($^2A_1$), as was claimed by Adamowicz and co-workers[25]. The DBS $^2A_1$, which is 0.054 eV above the VA (adiabatically) and is electronically bound at the equilibrium geometry of the neutral, may serve as a doorway state for electron capture. The calculations on benzonitrile solvated with one water molecule show that the VA is stabilized further and becomes bound even at the structure of the neutral complex. The calculations of photoelectron spectra show similar Franck–Condon envelops, blue-shifted by 0.39 eV with respect to the bare benzonitrile, also in excellent agreement with the experimental findings (0.32 eV) of Sanov and co-workers[24]. As was pointed out in the original experimental study[24], the similarity in the vibrational structure of the photodetachment spectra of the bare and microsolvated benzonitrile provides additional evidence that the ground state of benzonitrile is the valence $^2B_1$ state. This work highlights the importance of balanced and accurate treatment of electron correlation and the need to consider nuclear motion.

Acknowledgments:

This work has been supported in Los Angeles by the Army Research Office through grant W911NF-16-1-0232 and in Munich

by the German Research Foundation through grant JA2794/1-1 (Emmy Noether program). AIK is also a grateful recipient of the 2019 Simons Fellowship in Theoretical Physics, which supported her sabbatical stay in Germany.

Conflict of interests: A.I.K. is a member of directors and a part-owner of Q-Chem, Inc.

Notes and references

1 B. A. McGuire, A. M. Burkhardt, S. Kalenskii, C. N. Shingledecker, A. J. Remijan, E. Herbst and M. C. McCarthy, *Science*, 2018, **359**, 202–205.

2 J. E. Chiar, A. G. G. M. Tielens, A. J. Adamson and A. Ricca, *Astrophys. J.*, 2013, **770**, 78.

3 R. I. Kaiser, D. S. N. Parker and A. M. Mebel, *Annu. Rev. Phys. Chem.*, 2015, **66**, 43–67.

4 J. Simons, *J. Phys. Chem. A*, 2008, **112**, 6401–6511.

5 J. M. Herbert, *Rev. Comp. Chem.*, 2015, **28**, 391–517.

6 K. Jordan and F. Wang, *Annu. Rev. Phys. Chem.*, 2003, **54**, 367–396.

7 M. Gutowski, K. Jordan and P. Skurski, *J. Phys. Chem. A*, 1998, **102**, 2624–2633.

8 R. Fortenberry and T. D. Crawford, *J. Chem. Phys.*, 2011, **134**, 154304.

9 K. R. Lykke, R. D. Mead and W. C. Lineberger, *Phys. Rev. Lett.*, 1984, **52**, 2221–2224.

10 M. C. McCarthy, C. A. Gottlieb, H. Gupta and P. Thaddeus, *Astrophys. J. Lett.*, 2006, **652**, L141.

11 S. Brünken, H. Gupta, C. A. Gottlieb, M. C. McCarthy and P. Thaddeus, *Astrophys. J. Lett.*, 2007, **664**, L43.

12 P. Thaddeus, C. A. Gottlieb, H. Gupta, S. Brünken, M. C. McCarthy, M. Agúndez, M. Guelin and J. Cernicharo, *Astrophys. J.*, 2008, **677**, 1132.

13 Cernicharo, J., Guélin, M., Agúndez, M., Kawaguchi, K., McCarthy, M. and Thaddeus, P., *Astronomy & Astrophysics*, 2007, **467**, L37–L40.

14 J. Cernicharo, M. Guélin, M. Agundez, M. C. McCarthy and P. Thaddeus, *Astrophys. J. Lett.*, 2008, **688**, L83.

15 M. Agúndez, J. Cernicharo, M. Guélin, C. Kahane, E. Roueff, J. Kłos, F. Aoiz, F. Lique, N. Marcelino, J. R. Goicoechea, M. González-Garcia, C. Gottlieb, M. McCarthy and P. Thaddeus, *Astronomy & Astrophysics*, 2010, **517**, L2.

16 T. J. Millar, C. Walsh and T. A. Field, *Chem. Rev.*, 2017, **117**, 1765–1795.

17 K. Graupner, T. A. Field and G. C. Saunders, *Astrophys. J. Lett.*, 2008, **685**, L95.

18 F. Sebastianelli and F. A. Gianturco, *Eur. Phys. J. D*, 2012, **66**, 41.

19 F. Sebastianelli and F. A. Gianturco, *Eur. Phys. J. D*, 2010, **59**, 389–398.

20 N. Douguet, S. F. dos Santos, M. Raoult, O. Dulieu, A. E. Orel and V. Kokoouline, *J. Chem. Phys.*, 2015, **142**, 234309.

21 M. Khamesian, N. Douguet, S. F. dos Santos, O. Dulieu, M. Raoult, W. J. Brigg and V. Kokoouline, *Phys. Rev. Lett.*, 2016, **117**, 123001.

22 F. Carelli, F. A. Gianturco, R. Wester and M. Satta, *J. Chem. Phys.*, 2014, **141**, 054302.

23 W. Skomorowski, S. Gulania and A. I. Krylov, *Phys. Chem. Chem. Phys.*, 2018, **20**, 4805–4817.

24 A. R. Dixon, D. Khuseynov and A. Sanov, *J. Chem. Phys.*, 2015, **143**, 134306.

25 N. Kirnosov and L. Adamowicz, *Chem. Phys. Lett.*, 2017, **676**, 32–38.

26 W. E. Wentworth, L. W. Kao and R. S. Becker, *J. Phys. Chem.*, 1975, **79**, 1161–1169.

27 A. Zlatkis, C. K. Lee, W. E. Wentworth and E. C. M. Chen, *Anal. Chem.*, 1983, **55**, 1596–1599.

28 P. D. Burrow, A. E. Howard, A. R. Johnston and K. D. Jordan, *J. Chem. Phys.*, 1992, **96**, 7570–7578.

29 A. I. Krylov, *Annu. Rev. Phys. Chem.*, 2008, **59**, 433–462.

30 K. Sneskov and O. Christiansen, *WIREs: Comput. Mol. Sci.*, 2012, **2**, 566–584.

31 R. J. Bartlett, *WIREs: Comput. Mol. Sci.*, 2012, **2**, 126–138.

32 G. D. Purvis and R. J. Bartlett, *J. Chem. Phys.*, 1982, **76**, 1910–1918.

33 K. Raghavachari, G. . Trucks, J. A. Pople and M. Head-Gordon, *Chem. Phys. Lett.*, 1989, **157**, 479–483.

34 K. Emrich, *Nucl. Phys.*, 1981, **A351**, 379–396.

35 H. Sekino and R. J. Bartlett, *Int. J. Quant. Chem.*, 1984, **26**, 255–265.

36 H. Koch and P. Jørgensen, *J. Chem. Phys.*, 1990, **93**, 3333–3344.

37 H. Koch, H. Jensen, P. Jørgensen and T. Helgaker, *J. Chem. Phys.*, 1990, **93**, 3345–3350.

38 J. F. Stanton and R. J. Bartlett, *J. Chem. Phys.*, 1993, **98**, 7029–7039.

39 M. Nooijen and R. J. Bartlett, *J. Chem. Phys.*, 1995, **102**, 6735–6756.

40 S. V. Levchenko and A. I. Krylov, *J. Chem. Phys.*, 2004, **120**, 175–185.

41 A. I. Krylov, *Reviews in Comp. Chem.*, J. Wiley & Sons, 2017, vol. 30, pp. 151–224.

42 M. Nooijen and R. J. Bartlett, *J. Chem. Phys.*, 1995, **102**, 3629–3647.

43 D. A. Matthews and J. F. Stanton, *J. Chem. Phys.*, 2016, **145**, 124102.

44 T. C. Jagau, *J. Chem. Phys.*, 2018, **148**, 024104.

45 C. M. Oana and A. I. Krylov, *J. Chem. Phys.*, 2007, **127**, 234106–14.

46 C. M. Oana and A. I. Krylov, *J. Chem. Phys.*, 2009, **131**, 124114–15.

47 S. Gozem, A. O. Gunina, T. Ichino, D. L. Osborn, J. F. Stanton and A. I. Krylov, *J. Phys. Chem. Lett.*, 2015, **6**, 4532–4540.

48 J. Ortiz, *Adv. Quantum Chem.*, 1999, **35**, 33–52.

49 T.-C. Jagau and A. I. Krylov, *J. Chem. Phys.*, 2016, **144**, 054113.

50 E. Epifanovsky, D. Zuev, X. Feng, K. Khistyaev, Y. Shao and A. I. Krylov, *J. Chem. Phys.*, 2013, **139**, 134105.

51 X. Feng, E. Epifanovsky, J. Gauss and A. I. Krylov, *J. Chem. Phys.*, 2019, **151**, 014110.

52 V. A. Mozhayskiy and A. I. Krylov, *ezSpectrum*, ezSpectrum, http://iopenshell.usc.edu/downloads/.

53 S. Gozem and A. I. Krylov, *ezDyson User's Manual*, 2015, ezDyson, http://iopenshell.usc.edu/downloads/.

54 D. Zuev, T.-C. Jagau, K. B. Bravaya, E. Epifanovsky, Y. Shao, E. Sundstrom, M. Head-Gordon and A. I. Krylov, *J. Chem. Phys.*, 2014, **141**, 024102.

55 T.-C. Jagau, D. Zuev, K. B. Bravaya, E. Epifanovsky and A. I. Krylov, *J. Phys. Chem. Lett.*, 2014, **5**, 310–315.

56 T.-C. Jagau and A. I. Krylov, *J. Phys. Chem. Lett.*, 2014, **5**, 3078–3085.

57 T.-C. Jagau, D. B. Dao, N. S. Holtgrewe, A. I. Krylov and R. Mabbs, *J. Phys. Chem. Lett.*, 2015, **6**, 2786–2793.

58 Shao, Y.; Gan, Z.; Epifanovsky, E.; Gilbert, A.T.B.; Wormit, M.; Kussmann, J.; Lange, A.W.; Behn, A.; Deng, J.; Feng, X., et al., *Mol. Phys.*, 2015, **113**, 184–215.

59 A. I. Krylov and P. M. W. Gill, *WIREs: Comput. Mol. Sci.*, 2013, **3**, 317–326.

60 R. S. Mulliken, *J. Chem. Phys.*, 1955, **23**, 1997–2011.

61 C. Desfrancois, V. Periquet, Y. Bouteiller and J. P. Schermann, *J. Chem. Phys.*, 1998, **102**, 1274–1278.

62 T. Sommerfeld, *J. Phys. Chem. A*, 2004, **108**, 9150–9154.

63 H. L. d. C. J. H. Hendricks, S. A. Lyapustina and K. H. Bowen, *J. Chem. Phys.*, 1998, **108**, 8–11.

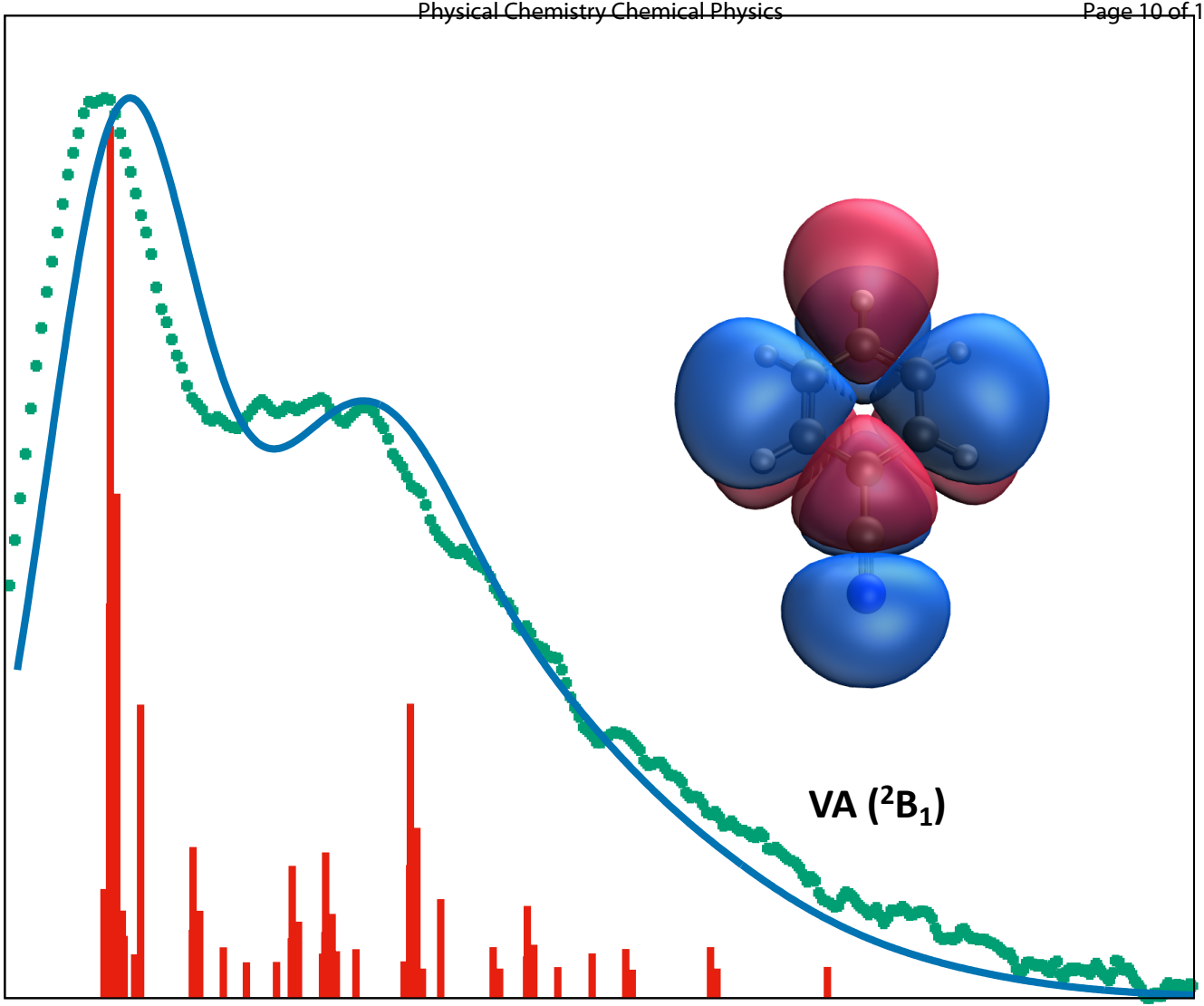
VA ($^2B_1$)